IEEE Access
Multidisciplinary ⋮ Rapid Review ⋮ Open Access Journal

Received April 23, 2022, accepted May 19, 2022, date of publication May 30, 2022, date of current version June 3, 2022.

Digital Object Identifier 10.1109/ACCESS.2022.3178847

Integration Design of Portable ECG Signal Acquisition With Deep-Learning Based Electrode Motion Artifact Removal on an Embedded System

YU-SYUAN JHANG[1], SZU-TING WANG[2], MING-HWA SHEU[1], SZU-HONG WANG[1], (Member, IEEE), AND SHIN-CHI LAI[3], (Member, IEEE)

[1]Department of Electronics Engineering, National Yunlin University of Science and Technology, Douliu 64002, Taiwan
[2]Doctor's Program of Smart Industry Technology Research and Design, National Formosa University, Huwei 632301, Taiwan
[3]Department of Automation Engineering, National Formosa University, Huwei 632301, Taiwan

Corresponding author: Shin-Chi Lai (shivan0111@nfu.edu.tw)

This work was supported in part by the Ministry of Science and Technology, Taiwan, under Grant MOST 110-2622-E-224-006, Grant 110-2221-E-150-045, and Grant 109-2221-E-150-043; in part by the Smart Machinery and Intelligent Manufacturing Research Center; in part by the Higher Education SPROUT Project, National Formosa University; and in part by the Ministry of Education (MOE) Female Researching Talent Cultivation Project for Science, Technology, Engineering, and Mathematics (STEM) field.

ABSTRACT For long-term electrocardiogram (ECG) signal monitoring, a portable and small size acquisition device with Bluetooth low energy (BLE) communication is designed and integrated with a Nvidia Jetson Xavier NX for realizing the electrode motion artifact removal technique. The digitalized ECG codes are converted from a front-end circuit, which contains several amplifiers and filters in the acquisition system. Thereafter, a zero padding scheme is applied for each 10-bits data to separate them into two-bytes data for BLE transmission. Xavier Edge AI platform receives these transmitted data and removes the electrode motion (EM) noise using the proposed low memory shortcut connection-based denoised autoencoder (LMSC-DAE). The simulation results demonstrate that the proposed algorithm significantly improves the signal-to-noise ratio (SNR) by 5.41 dB under the condition of $SNR_{in} = 12$ dB, compared with convolutional denoising autoencoder with long short-term memory (CNN-LSTM-DAE) method. For practical test, an Arduino DUE platform is employed to generate noise interference by controlling a commercial digital-to-analog convertor. By combining the proposed ECG acquisition device with a non-inverting weighted summer, it can be applied to verify the reproducibility of measurement for the proposed method. The measurement results clearly indicate that the proposed LMSC-DAE has a higher improvement of SNR and lower percentage root-mean-square difference than the state-of-the-art Fully Convolutional Denoising Autoencoder (FCN-DAE).

INDEX TERMS Electrocardiogram (ECG), ECG signal enhancement, embedded system, deep learning, denoising autoencoder (DAE).

I. INTRODUCTION

Electrocardiogram (ECG) is a common tool used to diagnosis, which records the electrical activity of the heart. By analysis, the ECG can help us check some important characterization, such as heart rhythm, heart rate variability, and sleeping stage. To enable the recording of ECG out-of-hospital, a wireless body area network (WBAN) device, Holter, has been developed in recent years. The Holter can be worn by a patient to record the ECG for a long-term period [1]. Also, these recorded data can be based on the diagnosis when the doctor examines the patient [2], [3]. The experiment in [4] reports a diagnostic accuracy could be improved if extended the monitoring period to 14 days, which revealed the demand for long-term monitoring [4]. However, some noise signals, such as baseline-wander (BW) noise, muscle artifacts (MA), and electrode motion (EM), are also recorded when the ECG signal is received, which may cause a doctor or an instrument to make an inaccurate diagnosis [5], [6].

Therefore, many ECG denoising algorithms have been implemented and can be classified into four categories: adaptive filter, empirical mode decomposition (EMD),

The associate editor coordinating the review of this manuscript and approving it for publication was Mohammad Zia Ur Rahman.

discrete wavelet transform (DWT), and denoising autoencoder (DAE). An adaptive filter is an algorithm that uses a filter whose coefficients change to an optimal state. The primary and reference signals are the inputs, and the reference signal is fed into a finite impulse response (FIR) filter or an infinite impulse response (IIR) filter. The filter output is used to approximately match the primary signal. Moreover, the adaptive filter adjusts its coefficients based on the difference between the primary and filtered reference signals using the stochastic gradient descent algorithm. In [7]–[9], a noisy ECG and reference signal were fed into an adaptive filter, and there was a high correlation between the reference and the noise in the noisy ECG. When the adaptive filter becomes stable, the filtered result is similar to the noise in the noisy ECG [10]. Consequently, the clean ECG signal can be estimated by calculating the difference between the noisy ECG and filtered reference signal. Nevertheless, a reference signal similar to a noisy ECG is not accessible in practice.

Using the empirical mode (EMD), the data can be decomposed into finite numbers of intrinsic mode functions (IMFs). The noise and IMFs of the ECG are segregated; accordingly, the clean ECG can be reconstructed by removing noise from the IMFs. In [11], a noisy ECG was decomposed into 15 IMFs. The last three IMFs can be regarded as BW noise, and the reconstructed signal is obtained after removing the BW noise. In [12], as corrupting noise possesses components primarily at high frequencies, a noisy ECG is decomposed into 11 IMFs. Soft thresholding is applied to retain the extrema of the time intervals between adjacent zero crossings. Consequently, noise is eliminated in the initial IMFs, and the signal content is mainly retained at higher levels of the IMFs, where the residual signal is the clean ECG. Hence, soft-thresholding is deployed to retain the larger values in the time interval between two adjacent zero crossings within an IMF; thus, high-frequency noise can be removed.

In another technique, the discrete wavelet transform (DWT) is a transform that is widely used in signal enhancement. In contrast to short-time Fourier transform (STFT), which divides the time-frequency space into an equally sized grid, DWT yields high-frequency resolution at low frequencies and high time resolution at high frequencies. In addition, a proper mother wavelet function is utilized to discretize the signal energy of the noise. Thereafter, either hard thresholding is applied to preserve the sharpness of the original ECG signal, or soft threshold is exploited to smoothen the reconstructed signal. In [13] and [14], the noisy ECG is transformed to the wavelet domain, and the denoising result is obtained using soft thresholding to remove the MA noise energy at a high frequency. In [15] and [16], both soft thresholding and hard thresholding were employed to remove MA and EM noises. In [17], various mother wavelets were utilized, whereas the effective mother wavelet was selected by cross-correlation to retain better ECG features.

Recently, deep-learning architectures have been extensively applied in various fields. Moreover, some denoising algorithms based on denoising autoencoder (DAE, [18]) have been proposed to reconstruct clean ECG signals. The DAE is extended from the autoencoder [19], which can be separated into encoder and decoder. The encoder was used to retain the features of the clean ECG signal, and the decoder was utilized to reconstruct the clean ECG signal using the features obtained from the encoder.

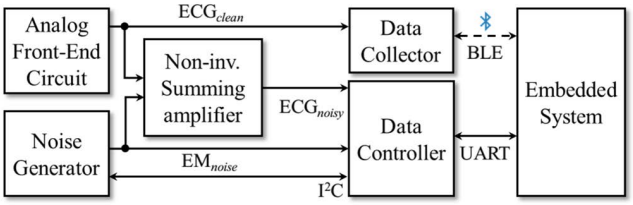

FIGURE 1. Block diagram of the proposed ECG signal acquisition and testing system with edge AI computation of EMAR.

In [20], the DAE architecture was applied to denoising ECG signals, and the result indicated that noises, including BW, MA, and EM, can be removed efficiently. In [21], the proposed work based on a fully convolutional denoising autoencoder (FCN-DAE) shows that a fully convolutional network can decrease the computation complexity and achieve superior denoising effects compared to the convolutional denoising autoencoder (CNN-DAE). In [22], a long short-term memory (LSTM) cell was added to the convolutional denoising autoencoder. The LSTM cell learns the sequential orders of ECG waves, which enhances the reconstruction quality. However, the high computational complexity restricts the implementation of the algorithm on an embedded system. Therefore, many denoising algorithms that attain better denoising effects than conventional algorithms have been proposed. However, an algorithm for removing the real measured noisy ECGs has not been developed in previous work, instead of simulated noisy ECGs.

In this study, a low-memory shortcut connection (LMSC)-based DAE was implemented on an embedded system. The DAE can extract the features more efficiently through the LMSC layer; thus, a smaller number of parameters and computational complexity are acquired to achieve denoising effects. Moreover, a test platform that can mix noise and ENG signals was designed to evaluate the denoising effects of various algorithms. Therefore, denoising results can be judged objectively. The results indicate that the proposed LMSC-DAE can remove noisy ECGs more effectively, and clean ECG signals can be recovered.

II. ARCHITECTURAL DESIGN OF PROPOSED SYSTEM AND NOISE SUPPRESSION TESTING PLATFORM

In this study, there are two main blocks in terms of the ECG signal acquisition system and the electrode motion artifact removal (EMAR) testing platform, as shown in Fig. 1. Continuous ECG signals in a static position (ECG_{clean}) can be acquired using a data collector (Atmega328p). After the zero-padding scheme, each 10-bit digitalized ECG code can be separated into two bytes for Bluetooth low energy (BLE)

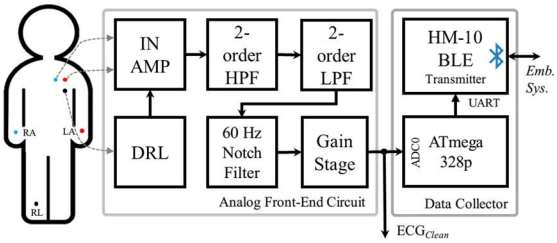

FIGURE 2. Flowchart of ECG signal sensing.

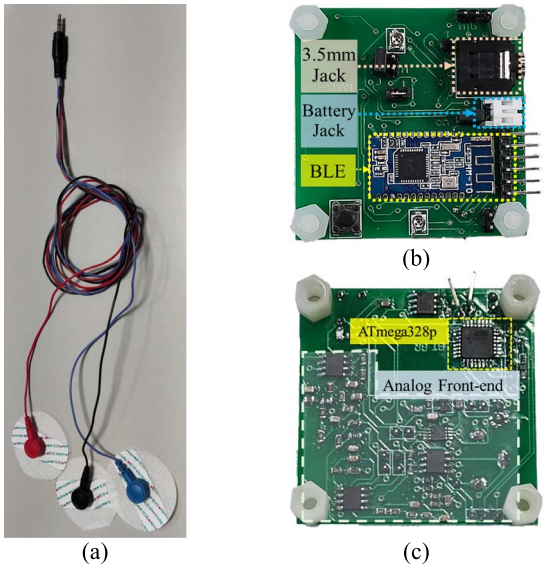

FIGURE 3. Proposed ECG signal acquisition device: (a) electrodes, (b) PCB top side, and (c) PCB bottom side.

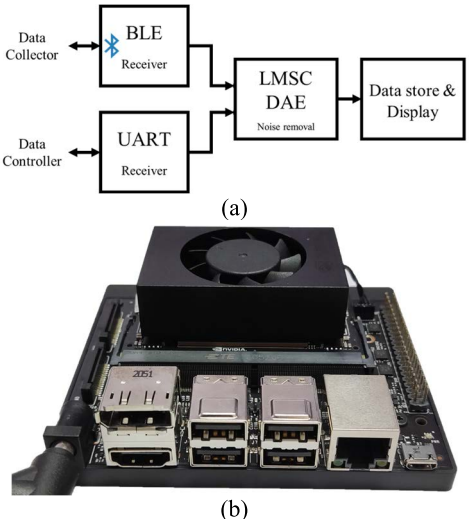

FIGURE 4. Edge AI embedded system: (a) workflow; (b) Jetson Xavier NX platform.

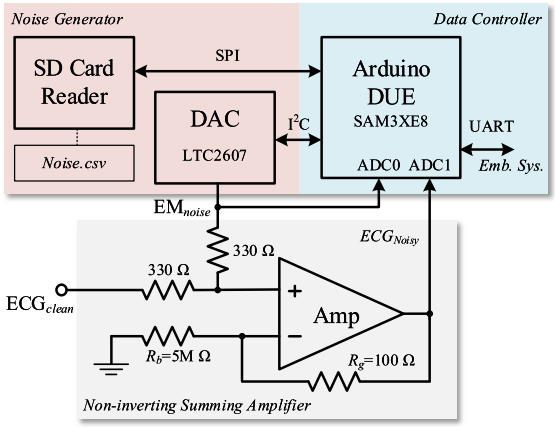

FIGURE 5. Block diagram of data control.

(HM-10) wireless transmission. Moreover, the transmitted data are received by the Xavier Edge AI platform, which is applied to remove motion artifact noise in real time. To test the performance of the EMAR algorithm, an Arduino DUE platform was used to control DAC (LTC2607) for EM noise generation (EM$_{noise}$). A non-inverting weighted summer was designed to generate the desired noisy ECG signals (ECG$_{noisy}$). Finally, the two-byte data were transmitted to an edge AI platform (Nvidia Jetson Xavier NX) via Universal Asynchronous Receiver/Transmitter (UART).

A. ECG SIGNAL SENSING

ECG signal sensing is primarily composed of an analog front-end circuit (AFEC) and a data collector with a BLE module, as shown in Fig. 2. The AFEC includes an instrumentation amplifier (INA333) with a driven right-leg circuit that provides a higher common-mode rejection ratio, which suppresses the common-mode signal interference from the power source. Following the suggestion of the American Heart Association [23], the frequency band of the proposed band-pass filter ranges from 0.05 to 150 Hz, and a notch filter is designed for the suppression of 60 Hz power-line interference. Finally, a gain stage amplifies the signal in the range of 0–3.3 V, which can be further sampled using an analog-to-digital converter (ADC).

The MCU is responsible for continuously processing the 10-bit digitalized ECG data at a sampling rate of 360 Hz, and it converts each code into two bytes for BLE data transmission. The data were transmitted to an embedded system of edge AI to execute the proposed EMAR algorithm in real time. For the proposed ECG signal acquisition device, all discrete components are weld on a 5 cm × 5 cm PCB, the system clock rate is set to 8 MHz, and the power consumption in measurement is approximately 81.4 mW, which is able to continuously monitor approximately 45.5 hours if a lithium battery with 3.7 V and 1 Ah is used. Fig. 3 shows the proposed ECG signal acquisition device.

B. SIGNAL PROCESSING AND TESTING ON AN EMBEDDED SYSTEM

For the data collection, an embedded system is employed to display the acquired signals on a screen and store them. Additionally, the noisy ECG was fed into the proposed EMAR

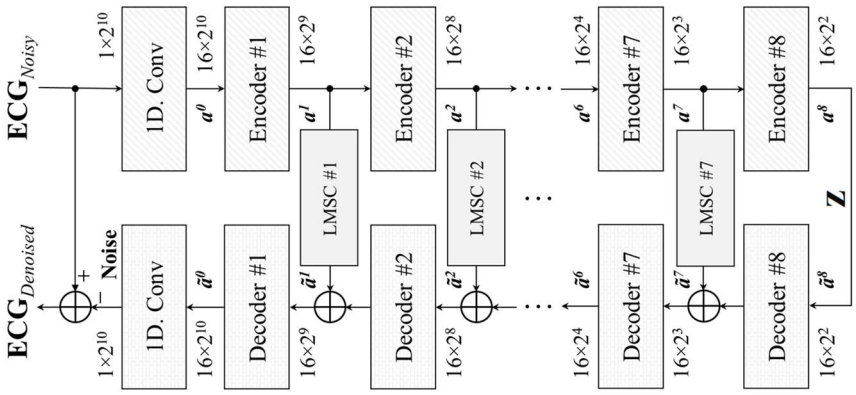

FIGURE 6. Overall neural architecture of the proposed LMCS-DAE.

algorithm every time while 1024 2-byte data from BLE were received. After completing EMAR, it yields the reconstructed denoised ECG data. Fig. 4 shows the workflow of the edge AI embedded system. For data control, an embedded system was applied to evaluate the performance of the proposed EMAR algorithm in real and practical cases. The noise generator, as shown in Fig. 5, is controlled by the Arduino DUE platform, and a 16-bit DAC generates EM noise according to the MIT-BIH noise stress test (NSTDB) [24], which is stored in an SD card. Thereafter, a non-inverting weighted summer was designed to mix both the human ECG signal and the desired EM noise into a noisy ECG signal. At this moment, the subjects remained in a static position as much as possible. Finally, the noisy ECG and EM noises are converted into digitalized codes and transmitted to the edge AI platform using the UART protocol.

III. PROPOSED LMSC-DAE DESIGN

The relationship between the noisy ECG, clean ECG, and MA noise is defined as (1). In this study, a lite EMAR algorithm, LMSC-DAE, was developed and can be easily implemented on an edge AI platform.

$$\mathrm{ECG}_{noisy} = \mathrm{ECG}_{clean} + \mathrm{MA}_{noise} \tag{1}$$

The proposed novel LMSC-DAE, shown in Fig. 6, comprises two convolution, eight encoder, eight decoder, and seven shortcut connection layers. To expand the feature maps to 16 × 1024, 1024 noisy ECG samples per frame were fed into one-dimension convolution layer (1D Conv.). Here, the channel size was fixed to 16 for all layers, and the feature size was 1024. The eight encoder layers extract the noise features ($\mathbf{a}^1$–$\mathbf{a}^8$), as shown in Fig. 7(a), and the feature size decreases per layer by a factor of two. In each encoder layer, a one-dimension residual block (1D Res.) is adopted to extract the noise feature and eliminate the vanishing gradient problem caused by layers of deep neural networks [25]. Additionally, it uses a one-dimensional convolution with stride = 2 to decrease the output features. Finally, the last encoder layer yields 16 × 4 compressed data, **z**.

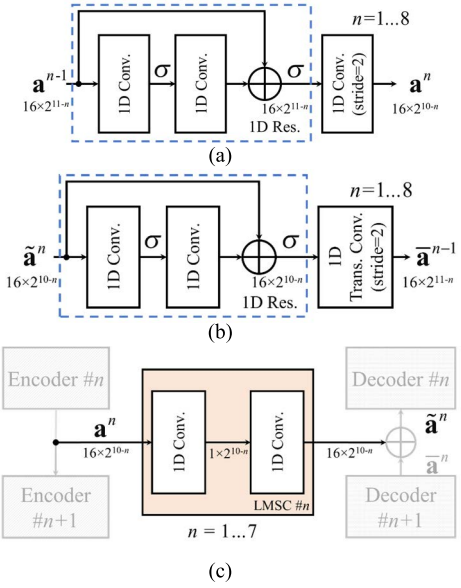

FIGURE 7. Workflow of the proposed LMSC-DAE: (a) encoder layer design, (b) decoder layer design, and (c) proposed LMSC layer design.

Conversely, the eight decoder layers reconstruct the noise, as shown in Fig. 7(b), and the feature size increases per layer by a factor of two. In each decoder layer, a one-dimension residual block (1D Res.) was adopted to reconstruct the noise, and one-dimensional transposed convolution (1D Trans. Conv.) with a stride of 2 was used to expand the output information. To enhance the learning effectiveness, each connection between the encoder and decoder layers inserts an extra layer, LMSC, to provide partial key information. The LMSC is used to improve the large amount of memory storage in use on the shortcut connection. Here, we used 1D. Conv. to compress the 16 channels feature information into one channel, and only $1 \times 2^{10-n}$ of data are reserved in memory. Thereafter, one channel feature is reproduced to obtain the original size of the feature data without including a non-linear function to avoid the problem of missing features [26]. After eight decoder layers, the size of the feature maps

recovers to 16 × 1024, and the signal is further fed into the last convolution layer, as shown in Fig. 7(c), to generate MA noise. Finally, the clean ECG signal can be computed by noisy ECG minus the reconstructed MA noise from the noisy ECG signal. Notably, kernel sizes of 1D Conv. and 1D Trans. Conv. were set to 5, and the activation function adopted LeakyReLU (slope = 0.1) to solve the dying ReLU problem [27].

IV. EXPERIMENTAL AND MEASUREMENT RESULTS

A. EVALUATION CRITERIA

To evaluate the noise cancellation performance, two criteria, the improvement of signal-to-noise ratio (SNR_{imp}) and percentage root-mean square (PRD), were used in this experiment. SNR_{imp} indicates the improvement in SNR from the reconstructed ECG (SNR_{out}) to the clean ECG (SNR_{in}). A greater SNR_{imp} indicates a better denoising capability, and it can be formulated as (2)–(4), where x_i, $\hat{x}_i$, and $\tilde{x}_i$, represent the value of clean ECG, noisy ECG, and reconstructed ECG with the sampled index i, respectively, and M represents the length of the input signal, which is 1024 in this study.

$$SNR_{imp} = SNR_{out} - SNR_{in} \tag{2}$$

$$SNR_{in} = 10 \times log_{10}\left(\frac{\sum_{i=0}^{M-1} x_i^2}{\sum_{i=0}^{M-1}(x_i - \hat{x}_i)^2}\right) \tag{3}$$

$$SNR_{out} = 10 \times log_{10}\left(\frac{\sum_{i=0}^{M-1} x_i^2}{\sum_{i=0}^{M-1}(x_i - \tilde{x}_i)^2}\right) \tag{4}$$

Here, PRD indicates the reconstructed quality of the output signal of the algorithm model by calculating the error between the clean and reconstructed ECGs. A smaller value of PRD corresponds to a smaller difference and is defined according to (5). To ensure fair evaluation, it is necessary to remove the bias in a clean ECG before evaluating the PRD value [28].

$$PRD(\%) = \sqrt{\frac{\sum_{i=0}^{M-1}(x_i - \tilde{x}_i)^2}{\sum_{i=0}^{M-1} x_i^2}} \times 100\% \tag{5}$$

B. DATASET FOR MODEL TRAINING AND PRE-PROCESSING

The MIT-BIH noise stress test (NSTDB) [24] was utilized to train various DAE models. The dataset includes 12 noisy ECG recordings and 3 raw recordings of the noise types (i.e., EM, BW, and MA) in a noisy ECG. All the records were sampled at 360 Hz and quantized using an 11-bit ADC. Noisy ECG recordings were generated by mixing two MIT-BIH arrhythmia database (MITDB) [29] ECG recordings (i.e., 118 and 119) with six different SNR values of EM (i.e., −6, 0, 6, 12, 18, and 24 dB). In this study, 12 noisy ECGs were separated into 6888 fragments with a length of 1024 samples. Thereafter, 80% of the fragments were split into a training set to train various DAE models, and the remaining 20% were used to evaluate SNR_{imp} and PRD. In the pre-processing, all fragments were first subtracted from the DC offset, and then they were divided by 2048 to normalize the fragment between -1 and 1.

TABLE 1. Number of MACs and trainable parameters for various DAEs.

Method	# of MACs	# of TPs
DNN	2.8M	1.39M
CNN	13.27M	1.11M
FCN [21]	25.08M	78,444
CNN-LSTM [22]	46.69M	10.96M
Proposed LMSC	12.36M	63,624

C. COMPARISONS OF COMPUTATIONAL COMPLEXITY AND TRAINABLE PARAMETERS FOR VARIOUS DAEs

To evaluate denoising performance, two well-known DAEs, namely, DNN-DAE and CNN-DAE, and two state-of-the-art approaches, namely, FCN-DAE [21] and CNN-LSTM-DAE [22], were compared with the proposed LMSC-DAE. The DNN-DAE consists of 10 fully connected layers, each with 512, 256, 128, 64, 32, 64, 128, 256, 512, and 1024 nodes. Meanwhile, the non-linear function, ReLU, was inserted in each fully connected layer. In CNN-DAE, six 1D Conv. layers were extracted, and the ECG features were compressed. Thereafter, six 1D Trans. Conv. and two fully connect layers accorded the extracted features to reconstruct a clean ECG. In FCN-DAE [21], there were seven 1D Conv. layers in the encoder to extract the features of the clean ECG. Subsequently, there were eight 1D Trans. Conv. layers in the decoder to reconstruct a clean ECG signal. The results demonstrated that the 1D Conv. and 1D Trans. Conv. used for all layers can effectively avoid magnitude distortion in the QRS complex wave. The CNN-LSTM-DAE [22] consists of eight 1D Conv. layers and one LSTM layer in the encoder. In the decoder, eight 1D Conv. layers, eight up-sampling layers, and one fully connected layer were used to obtain the reconstructed ECG. Thus, the CNN-LSTM-DAE [22] requires many multiply accumulate operations (MACs) and trainable parameters (TPs).

Table 1 compares the number of TPs and MACs in the three DAE models. The number of TPs of the CNN-LSTM-DAE is 158 times higher than that of the proposed LMSC-DAE, and it is not suitable for the implementation of an embedded system. In contrast to the FCN-DAE [21], the LMSC layer in the proposed model can pass the noise features from the encoder to the decoder more effectively. Therefore, the LMSC-DAE can use fewer MACs and trainable parameters to eliminate noise in noisy ECG, compared to the FCN-based DAE. The detailed information for each layer is summarized in Table 2. The proposed LMSC-DAE has 12.36M MACs and 1.45MB forward memory, and it is suitable for implementation in an embedded system for real-time operation. Moreover, 3888 trainable parameters are used in each encoder and decoder layer. The detailed layers of the residual block, encoder, decoder, and LMSC layers are listed in Table 3, and the kernel size and paddings are set to 5 and 2, respectively, in the entire LMSC-DAE.

TABLE 2. Layer information of the proposed LMSC-DAE.

Execution order - Annotation	Type	Operation	No. of filters × kernel size	Paddings	Region/ unit size	*AF	No. trainable parameter	Output size
0 – **Input (ECG_{noisy})**								1×2^{10}
1		Convolution	16 × 5	2	–	–	96	16×2^{10}
2	Encoder #1	Res. + Conv.(stride=2)	16 × 5	2	↓ 2	Leaky ReLU	3,888	16×2^{9}
4	Encoder #2	Res. + Conv.(stride=2)	16 × 5	2	↓ 2	Leaky ReLU	3,888	16×2^{8}
6	Encoder #3	Res. + Conv.(stride=2)	16 × 5	2	↓ 2	Leaky ReLU	3,888	16×2^{7}
8	Encoder #4	Res. + Conv.(stride=2)	16 × 5	2	↓ 2	Leaky ReLU	3,888	16×2^{6}
10	Encoder #5	Res. + Conv.(stride=2)	16 × 5	2	↓ 2	Leaky ReLU	3,888	16×2^{5}
12	Encoder #6	Res. + Conv.(stride=2)	16 × 5	2	↓ 2	Leaky ReLU	3,888	16×2^{4}
14	Encoder #7	Res. + Conv.(stride=2)	16 × 5	2	↓ 2	Leaky ReLU	3,888	16×2^{3}
16 – Code (z)	Encoder #8	Res. + Conv.(stride=2)	16 × 5	2	↓ 2	Leaky ReLU	3,888	$\mathbf{16 \times 2^{2}}$
17	Decoder #8	Res. + Trans. Conv.(stride=2)	16 × 5	2	↑ 2	Leaky ReLU	3,888	16×2^{3}
18	Decoder #7	Res. + Trans. Conv.(stride=2)	16 × 5	2	↑ 2	Leaky ReLU	3,888	16×2^{4}
19	Decoder #6	Res. + Trans. Conv.(stride=2)	16 × 5	2	↑ 2	Leaky ReLU	3,888	16×2^{5}
20	Decoder #5	Res. + Trans. Conv.(stride=2)	16 × 5	2	↑ 2	Leaky ReLU	3,888	16×2^{6}
21	Decoder #4	Res. + Trans. Conv.(stride=2)	16 × 5	2	↑ 2	Leaky ReLU	3,888	16×2^{7}
22	Decoder #3	Res. + Trans. Conv.(stride=2)	16 × 5	2	↑ 2	Leaky ReLU	3,888	16×2^{8}
23	Decoder #2	Res. + Trans. Conv.(stride=2)	16 × 5	2	↑ 2	Leaky ReLU	3,888	16×2^{9}
24	Decoder #1	Res. + Trans. Conv.(stride=2)	16 × 5	2	↑ 2	Leaky ReLU	3,888	16×2^{10}
25 – **Noise**		Convolution	16 × 5	2	–	–	81	1×2^{10}
26 – **Output ($ECG_{Denoised}$)**		**ECG_{Noisy} – Noise**						1×2^{10}
3 En. 1 → De. 1	LMSC #1	Conv. + Conv.	16 × 5	2	–	–	177	16×2^{9}
5 En. 2 → De. 2	LMSC #2	Conv. + Conv.	16 × 5	2	–	–	177	16×2^{8}
7 En. 3 → De. 3	LMSC #3	Conv. + Conv.	16 × 5	2	–	–	177	16×2^{7}
9 En. 4 → De. 4	LMSC #4	Conv. + Conv.	16 × 5	2	–	–	177	16×2^{6}
11 En. 5 → De. 5	LMSC #5	Conv. + Conv.	16 × 5	2	–	–	177	16×2^{5}
13 En. 6 → De. 6	LMSC #6	Conv. + Conv.	16 × 5	2	–	–	177	16×2^{4}
15 En. 7 → De. 7	LMSC #7	Conv. + Conv.	16 × 5	2	–	–	177	16×2^{3}
Total Trainable Parameters: 63,624		**Total MACs: 12.36 M**			**Forward/ Backward memory size: 1.45 MBytes**			

*AF: activation function; En.: encoder layer; De.: decoder layer; ↓: down-sampling; ↑: up-sampling

TABLE 3. Layer information of the submodule of the proposed LMSC-DAE.

Execution Order - Operation	No. filter × kernel size	Paddings	Region / unit size	*AF	No. trainable parameter	Input	Output
Residual Block (Res.)					**2,592**	**16 × N (g)**	**16 × N**
├ 1– 1D Convolution	16 × 5	2	–	Leaky ReLU	1,296	16 × N	16 × N
├ 2– 1D Convolution	16 × 5	2	–	–	1,296	16 × N	16 × N ($\bar{\mathbf{g}}$)
└ 3– Add ($\mathbf{g}+\bar{\mathbf{g}}$)	–	–	–	Leaky ReLU	–	16 × N	16 × N
Encoder Layer # (Res. + Conv.(stride=2))					**3,888**	**16 × N**	**16 × N/2**
├ 1– Residual Block	16 × 5	2	–	Leaky ReLU	1,296	16 × N	16 × N
└ 2– 1D Convolution (Stride=2)	16 × 5	2	↓ 2	–	–	16 × N	16 × N/2
Decoder Layer # (Res. + Trans. Conv.(stride=2))					**3,888**	**16 × N**	**16 × 2N**
├ 1– Residual Block	16 × 5	2	–	Leaky ReLU	2,592	16 × N	16 × N
└ 2– 1D Transpose Convolution (stride=2)	16 × 5	2	↑ 2	–	1,296	16 × N	16 × 2N
LMSC # (Conv. + Conv.)					**177**	**16 × N**	**16 × N**
├ 1– 1D Convolution	1 × 5	2	↓ 16	–	81	16 × N	1 × N
└ 2– 1D Convolution	16 × 5	2	↑ 16	–	96	1× N	16 × N

*AF: activation function; ↓: down-sampling; ↑: up-sampling

D. EXPERIMENTAL RESULTS OF NSTDB

In this study, the number of epochs for various DAEs was chosen to be 1000 to ensure that each model has suitable trainable parameters to remove the noise from noisy ECG. Fig. 8 presents the box plot of SNR_{imp} comparisons for various DAEs under the six SNR_{in} values for the testing set from NSTDB [24]. When the SNR_{in} is set to 6 dB, the noise signal is significantly greater than the clean ECG signal; thus, various DAEs have a significant improvement (average SNR_{imp} values approaching 20 dB) on the EMAR issue. However, the range of SNR_{imp} for various DAEs becomes limited when the noise becomes smaller with increasing SNR_{in} values. The results presented in Figs. 8 and 9 clearly show that the proposed LMSC-DAE with lower MACs and fewer TPs has the best SNR_{imp} and *PRD* values compared to other approaches. The CNN-LSTM-DAE [22] reported better performance, whereas the clean signal was corrupted by additive Gaussian white noise at specified SNR levels of −1, 3, and

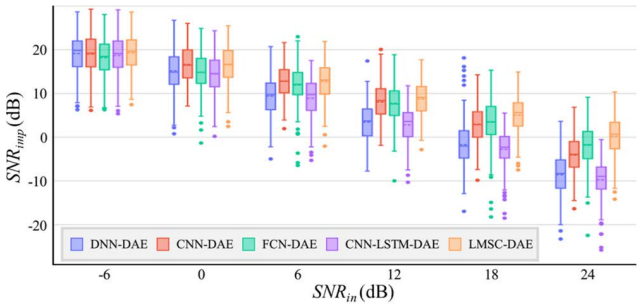

FIGURE 8. Box plots for SNR_{imp} comparison of various DAEs with six different SNR_{in} values under the testing set of NSTDB; the box plots include outliers (dot), minimum, interquartile range, median, maximum, and average (dotted line).

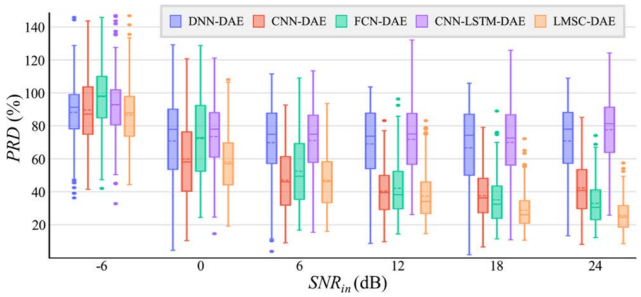

FIGURE 9. Box plots for *PRD* comparison of various DAEs with six different SNR_{in} values under the testing set of NSTDB; the box plots include outliers (dot), minimum, interquartile range, median, maximum, and average (dotted line).

TABLE 4. SNR_{imp} comparison of various DAEs in NSTD.

DAE Methods	SNR_{in} (dB)					
	-6	0	6	12	18	24
DNN	18.85	15.20	9.41	3.48	-1.66	-8.53
CNN	18.80	16.64	12.83	8.06	2.99	-4.06
FCN [21]	18.22	14.82	11.95	7.75	3.51	-1.80
CNN-LSTM [22]	18.71	14.53	8.94	2.83	-2.69	-9.65
Proposed	**19.30**	**16.57**	**12.74**	**8.78**	**4.10**	**0.70**

TABLE 5. *PRD* comparison of various DAEs in NSTDB.

DAE Methods	SNR_{in} (dB)					
	-6	0	6	12	18	24
DNN	87.09	70.69	69.74	68.95	66.57	70.68
CNN	89.54	58.03	46.98	40.24	37.49	42.19
FCN [21]	97.67	72.20	52.39	42.07	34.92	32.81
CNN-LSTM [22]	92.90	73.38	71.01	71.71	69.83	77.59
Proposed	**86.04**	**57.88**	**46.89**	**37.18**	**28.68**	**25.47**

7 dB for the training and testing sets. However, it showed nonsignificant improvement in this work under different SNR levels of MA noise. Therefore, the results indicate that the CNN-LSTM-DAE [22] may not be effective in eliminating MA noise.

The average criteria for SNR_{imp} and *PRD* are listed in Tables 4 and 5, respectively. The results demonstrate that the SNR_{imp} achieved a significant improvement for all models when the SNR_{in} is -6, 0, and 6 dB. However, when the level of noise was quite low ($SNR_{in} = 24$ dB and 18 dB), only LMSC-DAE had positive SNR_{imp} values. In the performance of *PRD*, the proposed LMSC-DAE has a 2.3% improvement over the other approaches when $SNR_{in} = -6$ dB. Additionally, the reconstructed ECG is much closer than the clean ECG when the level of noise is smaller. In contrast, CNN-LSTM-DAE exhibited [22] the worst *PRD* for any SNR_{in}.

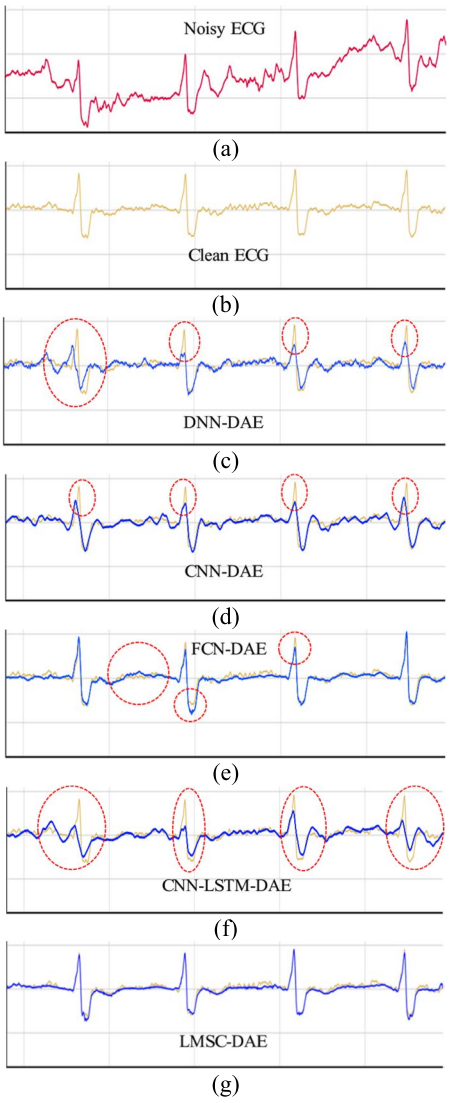

FIGURE 10. Comparison of the reconstructed results for NSTDB: (a) noisy ECG (Input); (b) clean ECG (Ground truth); (c) DNN-DAE; (d) CNN-DAE; (e) FCN- DAE; (f) CNN-LSTM-DAE; (g) LMSC-DAE.

Fig. 10 shows the noise-removal experiment for one fragment in the testing set. As shown in Fig. 10(a), it is difficult to recognize the ECG features in the noisy ECG because of the noise covering the clean ECG in Fig. 10(b). The results in Figs. 10(c) and 10(d) demonstrate that the waves of the QRS complex are distorted in both DNN-DAE and CNN-DAE. Fig. 10(e) reveals that the FCN-DAE [21] output can remove most of the noise, but it is not perfect owing to the incorrect detection in the marked location. Fig. 10(f) shows that most

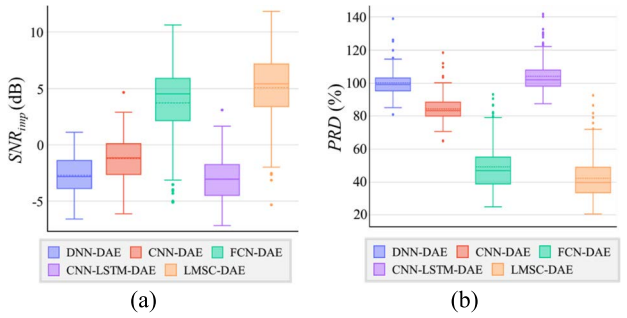

FIGURE 11. Box plots of the denoising criteria of three DAEs under six SNR_{in} for the 8 volunteer's 5-min ECG recordings: (a) comparison of SNR_{imp}; (b) comparison of *PRD*.

of the ECG features are distorted in CNN-LSTM-DAE [22], and Fig. 10(g) shows that the proposed method can retain the ECG features and eliminate the noise more effectively than other approaches.

V. MEASUREMENT RESULTS OF THE VOLUNTEER's ECG SIGNALS

In this study, the proposed testing platform is utilized to record the desired real-time noisy ECG, which is mixed with the given MA noises and human ECG signals. Thereafter, noisy ECG signals were further applied to evaluate the performance of noise removal for various DAEs. Ideally, it would be better to collect noisy ECG signals from volunteers. However, it is impossible to evaluate SNR_{imp} and *PRD* because we cannot obtain the clean ECG and the corresponding noisy ECG simultaneously. To perform an objective evaluation [30], clean ECG recordings were obtained from the volunteers, which were kept in a static position. Meanwhile, a 16-bit DAC (LT2607) controlled by the Arduino DUE platform directly generated EM noise. Fig. 11 shows the box plots of SNR_{imp} and *PRD* for various DAEs under the condition of real-time recordings of the volunteer's ECG. There were eight ECG recordings, each of which took 5 minutes. Because the volunteer's ECG belonged to unseen and untrained patterns, the testing results would be more suitable for practical applications. Table 6 summarizes the detailed average SNR_{imp} and *PRD* of various DAEs under 8 the 5-min ECG recordings of volunteer. The results indicate that all DAEs have an different performance between the NSTDB experiment and the volunteer's ECG recordings. Considering the NSTDB experiment, the DAEs have sufficient data to learn the features of EM noise in the training phase; thus, FCN-DAE [21] and the proposed algorithm can reconstruct the clean ECG effectively in the testing phase. In contrast, none of the volunteer's ECG recordings were observed in the training phase. Therefore, the testing sets using the experiment of NSTDB can obtain better improvement. Overall, the proposed LMSC-DAE with lower computational complexity can achieve an SNR_{imp} of 5.41 dB and *PRD* of 42.31% on average. Therefore, it is a much better solution for an embedded system in implementation.

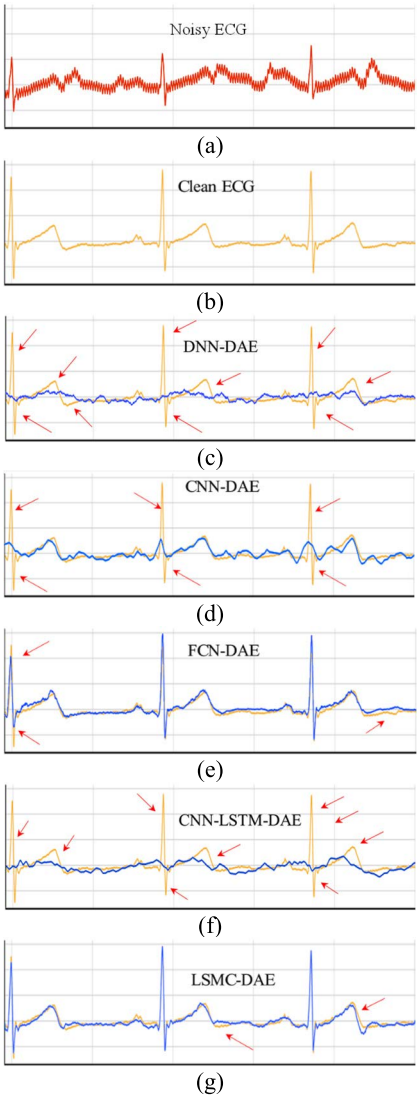

FIGURE 12. Comparison of the reconstructed results for volunteer's ECG recordings: (a) Noisy ECG (Input); (b) clean ECG (Ground truth); (c) DNN-DAE; (d) CNN-DAE; (e) FCN- DAE; (f) CNN-LSTM-DAE; (g) LMSC-DAE.

TABLE 6. Comparison of SNR_{imp} and *PRD* for volunteer's ECG recordings.

DAE Methods	SNR_{imp} (dB)	*PRD* (%)
DNN	-2.70	100.02
CNN	-1.21	84.25
FCN [21]	3.72	49.20
CNN-LSTM [22]	-3.04	102.5
Proposed LMSC	5.41	42.31

Fig. 12 shows the noise-removal experiment for one fragment in the volunteer's ECG recordings. Figs. 12(c) and 12(f) reveal that DNN-DAE and CNN-LSTM-DAE [22] were unable to extract the effective features to reconstruct the ECG when the ECG was never observed before. Fig. 12(d) demonstrates that the CNN-DAE was able to reconstruct the T wave only. FCN-DAE [21], as shown in Fig. 12(e), and LMSC-DAE, as shown in Fig. 12(g), clearly show better

denoising results in this experiment, although FCN-DAE [21] reconstructs an incorrect wave in the marked location.

VI. DISCUSSION

Based on the experiments and measurement results, DNN-DAE, CNN-DAE, and CNN-LSTM-DAE [22], which used a fully connected layer, were unable to reconstruct an ECG from the volunteer's ECG. In the NSTDB experiment, because the ECG features of the testing and training sets were similar, three DAEs could maintain the ECG features by fully connected layer. However, the large number of training parameters causes the neural network to not efficiently exclude unnecessary features. Thus, it is easy to lose robustness when the neural network faces the outlier data, such as the experiment of the volunteer's ECG. Conversely, the FCN-DAE [21] and proposed LMSC-DAE consist only of convolutional layers and activation functions. It is efficient to extract features using a convolution layer in a time series. Moreover, the LMSC layer passes partial key features between the encoder and decoder, and the experimental results demonstrate a better noise suppression ability in practical applications of ECG signal processing.

A. CONCLUSION

In this paper, a signal acquisition system with a deep-learning-based LMSC-DAE was proposed for human ECG records, as well as EM noise suppression. The EM noise was randomly generated from the NSTDB with specified SNR levels of −6, 0, 6, 12, 18, and 24 dB. The proposed LMSC-DAE can achieve a higher SNR_{imp} and lower *PRD* than other related approaches, whether the input ECG signal is given from the MITDB or acquired from a volunteer. Considering the applications of edge AI computing, the proposed design is very useful for the restricted computation capability to execute the deep-learning-based noise-suppression algorithm and to obtain better denoised ECG signals in the future.

REFERENCES

[1] C. A. Tavera, J. H. Ortiz, O. I. Khalaf, D. F. Saavedra, and T. H. H. Aldhyani, "Wearable wireless body area networks for medical applications," *Comput. Math. Methods Med.*, vol. 2021, pp. 1–9, Apr. 2021, doi: 10.1155/2021/5574376.

[2] M. Hadjem, O. Salem, and F. Nait-Abdesselam, "An ECG monitoring system for prediction of cardiac anomalies using WBAN," in *Proc. IEEE 16th Int. Conf. e-Health Netw., Appl. Services (Healthcom)*, Oct. 2014, pp. 441–446, doi: 10.1109/HEALTHCOM.2014.7001883.

[3] M. A. Serhani, H. T. E. Kassabi, H. Ismail, and A. Nujum Navaz, "ECG monitoring systems: Review, architecture, processes, and key challenges," *Sensors*, vol. 20, no. 6, p. 1796, Mar. 2020, doi: 10.3390/S20061796.

[4] S.-K. Chua, L.-C. Chen, L.-M. Lien, H.-M. Lo, Z.-Y. Liao, S.-P. Chao, C.-Y. Chuang, and C.-Z. Chiu, "Comparison of arrhythmia detection by 24-hour Holter and 14-day continuous electrocardiography patch monitoring," *Acta Cardiol. Sinica*, vol. 36, no. 3, p. 251, 2020, doi: 10.6515/ACS.202005_36(3).20190903A.

[5] Z. F. Apandi, R. Ikeura, S. Hayakawa, and S. Tsutsumi, "An analysis of the effects of noisy electrocardiogram signal on heartbeat detection performance," *Bioengineering*, vol. 7, no. 2, pp. 1–15, Jun. 2020, doi: 10.3390/BIOENGINEERING7020053.

[6] M. D'Aloia, A. Longo, and M. Rizzi, "Noisy ECG signal analysis for automatic peak detection," *Information*, vol. 10, no. 2, p. 35, Jan. 2019, doi: 10.3390/INFO10020035.

[7] M. Milanesi, N. Martini, N. Vanello, V. Positano, M. F. Santarelli, R. Paradiso, D. De Rossi, and L. Landini, "Multichannel techniques for motion artifacts removal from electrocardiographic signals," in *Proc. Int. Conf. IEEE Eng. Med. Biol. Soc.*, Aug. 2006, pp. 3391–3394, doi: 10.1109/IEMBS.2006.260464.

[8] M. Z. U. Rahman, R. A. Shaik, and D. V. R. K. Reddy, "Efficient and simplified adaptive noise cancelers for ECG sensor based remote health monitoring," *IEEE Sensors J.*, vol. 12, no. 3, pp. 566–573, Mar. 2012.

[9] M. Z. U. Rahman, G. V. S. Karthik, S. Y. Fathima, and A. Lay-Ekuakille, "An efficient cardiac signal enhancement using time–frequency realization of leaky adaptive noise cancelers for remote health monitoring systems," *Measurement*, vol. 46, no. 10, pp. 3815–3835, Dec. 2013.

[10] S. Haykin and B. Widrow, *Least-Mean-Square Adaptive Filters*. Hoboken, NJ, USA: Wiley, Jan. 2005, doi: 10.1002/0471461288.

[11] N. Pan, V. Mang, M. P. Un, and P. S. Hang, "Accurate removal of baseline wander in ECG using empirical mode decomposition," in *Proc. Joint Meeting 6th Int. Symp. Noninvasive Funct. Source Imag. Brain Heart Int. Conf. Funct. Biomed. Imag. (NFSI ICFBI)*, Oct. 2007, pp. 177–180, doi: 10.1109/NFSI-ICFBI.2007.4387719.

[12] S. Samadi and M. B. Shamsollahi, "ECG noise reduction using empirical mode decomposition based on combination of instantaneous half period and soft-thresholding," in *Proc. 2nd Middle East Conf. Biomed. Eng.*, Feb. 2014, pp. 244–248, doi: 10.1109/MECBME.2014.6783250.

[13] C. Sawant and H. T. Patii, "Wavelet based ECG signal de-noising," in *Proc. 1st Int. Conf. Netw. Soft Comput. (ICNSC)*, Aug. 2014, pp. 20–24, doi: 10.1109/CNSC.2014.6906684.

[14] H.-Y. Lin, S.-Y. Liang, Y.-L. Ho, Y.-H. Lin, and H.-P. Ma, "Discrete-wavelet-transform-based noise removal and feature extraction for ECG signals," *IRBM*, vol. 35, no. 6, pp. 351–361, Dec. 2014, doi: 10.1016/J.IRBM.2014.10.004.

[15] J. Zhang, J.-L. Lin, X.-L. Li, and W.-Q. Wang, "ECG signals denoising method based on improved wavelet threshold algorithm," in *Proc. IEEE Adv. Inf. Manage., Communicates, Electron. Autom. Control Conf. (IMCEC)*, Oct. 2016, pp. 1779–1784, doi: 10.1109/IMCEC.2016.7867525.

[16] S. Zhang, J. Gao, J. Yang, and S. Yu, "A Mallat based wavelet ECG de-noising algorithm," *Appl. Mech. Mater.*, vols. 263–266, pp. 2267–2270, Feb. 2013, doi: 10.4028/WWW.SCIENTIFIC.NET/AMM.263-266.2267.

[17] B. N. Singh and A. K. Tiwari, "Optimal selection of wavelet basis function applied to ECG signal denoising," *Digit. Signal Process.*, vol. 16, no. 3, pp. 275–287, May 2006, doi: 10.1016/J.DSP.2005.12.003.

[18] P. Vincent, H. Larochelle, I. Lajoie, Y. Bengio, and P.-A. Manzagol, "Stacked denoising autoencoders: Learning useful representations in a deep network with a local denoising criterion," *J. Mach. Learn. Res.*, vol. 11, no. 12, pp. 3371–3408, Dec. 2010.

[19] J. Schmidhuber, "Deep learning in neural networks: An overview," *Neural Netw.*, vol. 61, pp. 85–117, Oct. 2014, doi: 10.1016/j.neunet.2014.09.003.

[20] P. Xiong, H. Wang, M. Liu, and X. Liu, "Denoising autoencoder for eletrocardiogram signal enhancement," *J. Med. Imag. Health Inform.*, vol. 5, no. 8, pp. 1804–1810, Dec. 2015.

[21] H.-T. Chiang, Y.-Y. Hsieh, S.-W. Fu, K.-H. Hung, Y. Tsao, and S.-Y. Chien, "Noise reduction in ECG signals using fully convolutional denoising autoencoders," *IEEE Access*, vol. 7, pp. 60806–60813, 2019.

[22] E. Dasan and I. Panneerselvam, "A novel dimensionality reduction approach for ECG signal via convolutional denoising autoencoder with LSTM," *Biomed. Signal Process. Control*, vol. 63, Jan. 2021, Art. no. 102225.

[23] P. Kligfield, L. S. Gettes, J. J. Bailey, R. Childers, B. J. Deal, E. W. Hancock, G. van Herpen, J. A. Kors, P. Macfarlane, D. M. Mirvis, O. Pahlm, P. Rautaharju, and G. S. Wagner, "Recommendations for the standardization and interpretation of the electrocardiogram: Part I: The electrocardiogram and its technology: A scientific statement from the American Heart Association Electrocardiography and Arrhythmias Committee, Council on Clinical Cardiology; the American College of Cardiology Foundation; and the Heart Rhythm Society," *Circulation*, vol. 115, no. 10, pp. 1306–1324, Mar. 2007, doi: 10.1161/CIRCULATIONAHA.106.180200.

[24] G. Moody and R. Mark. *MIT-BIH Noise Stress Test Database V1.0.0*. Accessed: Mar. 1, 2022. [Online]. Available: https://physionet.org/content/nstdb/1.0.0/

[25] K. He, X. Zhang, S. Ren, and J. Sun, "Deep residual learning for image recognition," in *Proc. IEEE Conf. Comput. Vis. Pattern Recognit. (CVPR)*, Jun. 2016, pp. 770–778.

[26] J. Lin, W.-M. Chen, H. Cai, C. Gan, and S. Han, "MCUNetV2: Memory-efficient patch-based inference for tiny deep learning," Oct. 2021, *arXiv:2110.15352*.
[27] A. L. Maas, A. L. Maas, A. Y. Hannun, and A. Y. Ng, "Rectifier nonlinearities improve neural network acoustic models," in *Proc. ICML Workshop Deep Learn. Audio, Speech Lang. Process.*, 2013, p. 3.
[28] A. Němcová, R. Smíšek, L. Maršánová, L. Smital, and M. Vítek, "A comparative analysis of methods for evaluation of ECG signal quality after compression," *BioMed Res. Int.*, vol. 2018, pp. 1–26, Jul. 2018.
[29] G. Moody and R. Mark. *MIT-BIH Arrhythmia Database V1.0.0*. Accessed: Mar. 1, 2022. [Online]. Available: https://physionet.org/content/mitdb/1.0.0/
[30] L. Galeotti, L. Johannesen, J. Vicente, and D. G. Strauss, "Measurement of noise in ECG signals to improve automatic delineation," in *Proc. Comput. Cardiol.*, 2013, pp. 511–514.

YU-SYUAN JHANG was born in Keelung, Taiwan, in 1993. He received the B.S. degree from the Department of Computer Science and Information Engineering, Nanhua University, Chiayi County, Taiwan, in 2014, and the M.S. degree from the Institute of Medical Science and Technology, National Sun Yat-sen University, Kaohsiung, Taiwan. He is currently pursuing the Ph.D. degree with the Department of Electronic Engineering, National Yunlin University of Science and Technology, Yunlin County, Taiwan. His research interests include digital signal processing, embedded system application, FPGA application design, android application design, deep learning, and adaptive filter algorithm.

SZU-TING WANG received the B.S. degree from the Department of Computer Science and Information Management, Providence University, Taichung, Taiwan, and the M.S. degree from the Department of Information Engineering and Computer Science, Feng Chia University, Taichung. She is currently pursuing the Ph.D. degree with the Ph.D. Program of Smart Industry Technology Research and Design, National Formosa University, Yunlin, Taiwan. Her research interests include image processing, digital signal processing, and deep learning.

MING-HWA SHEU received the M.S. and Ph.D. degrees in electrical engineering from National Cheng Kung University, Tainan, Taiwan, in 1989 and 1993, respectively. He is currently a Full Professor with the Department of Electronic Engineering, National Yunlin University of Science and Technology, Yunlin, Taiwan. His research interests include CAD/VLSI, digital signal process, algorithm analysis, and embedded systems. From 2015 to 2018, he was a Supervisor at the Taiwan IC Design Association. He was a Committee Chair of the E.E. Course Planning For Technical High School, Ministry of Education, Taiwan. He was a Review Committee of the Engineering Department, Ministry of Science and Technology (MOST). From 2008 to 2011, he was the Chairperson of the Department of Electronic Engineering.

SZU-HONG WANG (Member, IEEE) received the M.S. degree from the Department of Computer and Communication Engineering, National Kaohsiung University of Science and Technology, Kaohsiung, Taiwan, in 2005, and the Ph.D. degree from the Institute of Engineering Science and Technology, National Kaohsiung First University of Science and Technology, in 2010. He is currently an Associate Professor with the Bachelor Program in Interdisciplinary Studies, National Yunlin University of Science and Technology. His main research interests include image processing, DSP/VLSI architecture design, and embedded systems.

SHIN-CHI LAI (Member, IEEE) was born in Taichung, Taiwan, in 1980. He received the B.S. degree in electronic engineering from Chienkuo Technology University, Changhua, Taiwan, in 2002, the M.S. degree in electronic engineering from the National Yunlin University of Science and Technology, Yunlin, Taiwan, in 2005, and the Ph.D. degree from National Cheng Kung University, Tainan, Taiwan, in 2011. From October 2011 to July 2013, he was an Assistant Research Fellow at the Department of Electrical Engineering, National Cheng Kung University. From August 2013 to July 2016, he was an Assistant Professor at the Department of Computer Science and Information Engineering, Nanhua University. From August 2016 to July 2019, he was an Associate Professor at the Department of Computer Science and Information Engineering. From August 2019 to July 2021, he was a Full Professor at the Department of Computer Science and Information Engineering, Nanhua University, Chiayi, Taiwan. Currently, he is a Professor with the Department of Automation Engineering, National Formosa University. His main research interests include signal processing and its circuit design, especially for speech, audio, biomedical, and multimedia applications.